1-1-2004

# Analysis of a Phase Change Energy Storage System for Pulsed Power Dissipation

S Krishnan

S V. Garimella
*Purdue University*, sureshg@purdue.edu



Krishnan, S and Garimella, S V., "Analysis of a Phase Change Energy Storage System for Pulsed Power Dissipation" (2004). *CTRC Research Publications.* Paper 75.
http://dx.doi.org/10.1109/TCAPT.2004.825758

# Analysis of a Phase Change Energy Storage System for Pulsed Power Dissipation[†]

Shankar Krishnan and Suresh V. Garimella[‡]
Cooling Technologies Research Center
School of Mechanical Engineering
Purdue University, West Lafayette, Indiana 47907-2088

## ABSTRACT

The melting of a phase change material in a container of rectangular cross-section with multiple discrete heat sources mounted on one side is investigated for electronics cooling by latent heat energy storage. This numerical study focuses on the thermal management issues that arise when electronic components experience sudden surges in power dissipation. The transient response of the energy storage system to short pulses in power dissipation is studied. Convective cooling using air-cooled heat sinks on the sides of the containment remote from the heat sources provides for heat rejection to ambient air. The analysis is performed under different pulse frequencies. Different aspect ratios for the containment volume as well as different locations for the heat sources are studied in order to identify an optimal arrangement. Conduction and convection in the phase change material as well as conduction through the containment walls are considered in the computations. The constitutive equations are implicitly solved using a fully transient method on fixed orthogonal co-located finite volumes. The system is characterized based on the rate of heat absorption as well as the maximum temperatures experienced at the heat sources. Improvements that can be made in the application of latent heat energy storage to electronics cooling applications are discussed based on the results from the present study.

KEYWORDS: phase change energy storage, transient heat dissipation, electronics cooling, pulsed power, phase change material

---

[†] Submitted for publication in *IEEE CPMT*, August, 2002, and in revised form, June 2003.

[‡] Author to whom correspondence should be addressed: Tel: (765) 494-5621; sureshg@ecn.purdue.edu

## NOMENCLATURE

| | |
|---|---|
| A | Apparent heat capacity, equation (3) |
| $C_p$ | Specific heat capacity, J $kg^{-1}K^{-1}$ |
| $f_l$ | Volume fraction |
| g | Acceleration due to gravity, m $s^{-2}$ |
| H | Height of the container, m |
| h | Heat transfer coefficient, W $m^{-2}$ $K^{-1}$ |
| K | Constant, equation (2) |
| k | Thermal conductivity, W $m^{-1}K^{-1}$ |
| p | Pressure, $Nm^{-2}$ |
| Q | Heat energy, J |
| T | Temperature, K |
| t | Time, seconds |
| U | Velocity, m $s^{-1}$ |
| u,v | Velocity in x and y directions, m $s^{-1}$ |
| W | Width of the container, m |
| x,y | Cartesian coordinates |

*Greek symbols*

| | |
|---|---|
| $\alpha$ | Thermal diffusivity $m^2$ $s^{-1}$ |
| $\beta$ | Thermal expansion coefficient, $K^{-1}$ |
| $\Delta H$ | Enthalpy of freezing, J $kg^{-1}$ |
| $\Delta t$ | Time step |
| $\Delta x, \Delta y$ | Spatial mesh sizes, m |
| $\mu$ | Kinematic viscosity, $m^2$ $s^{-1}$ |
| $\rho$ | Density, kg $m^{-3}$ |

*Subscripts*

| | |
|---|---|
| o | Initial condition |
| abs | Absorbed |

| | |
|---|---|
| eff | Effective property |
| l | Liquid |
| s | Solid |

*Superscripts*

| | |
|---|---|
| ~ | Unit vector |

## 1. INTRODUCTION

The use of phase change materials (PCMs) for electronics thermal management is receiving increased attention due to the passive nature of this approach. The storage of thermal energy in the form of latent heat in the PCM is exploited, resulting in a compact cooling system.

For steady-state applications, desirable characteristics of a PCM [1] include a high latent heat of fusion, high density (to reduce the containment volume), and a high specific heat. For transient applications, where the thermal response of the material is critical, a high latent heat of fusion and high thermal diffusivity of the material are desirable. The melting temperature of a PCM is also very important in determining its suitability for use in a given application.

Inorganic PCMs generally have a volumetric latent heat storage capacity that is twice that of organic compounds [1]. However, organic PCMs such as alkanes and paraffins generally have the advantages of melting congruently, of self-nucleation, and of being non-corrosive to conventional materials. A detailed discussion of choices for PCMs is available in [1,2].

While phase change energy storage has been extensively studied for solar energy applications [2,3], its use in the thermal management of electronics is being investigated only more recently. Ishizuka and Fukuoka [4] investigated a low melting point metallic PCM (Bi/Pb/Sn/In) and found experimentally that the operating temperature rise of the substrate could be suppressed for a significant amount of time. Baker et al. [5] performed a conduction-only

analysis of the thermal performance of a heterogeneous package. Periodic heating was considered and two nonmetallic PCMs (octadecane and pentacosane) were used for heat storage with metal fins to enhance the effective thermal conductivity. Peak operating temperatures, energy storage rates in the package and the PCM were reported. Pal and Joshi [6] performed a numerical analysis of the melting of an organic PCM under a constant power input for passive thermal control of a plastic quad flat package. Transient variations in the power input were considered in [7] for passive thermal control of electronic modules. Alawadhi and Amon [8] used a conduction analysis to compare the performance of a PCM thermal control unit, with and without a thermal conductivity enhancer (TCE) included in the domain.

Vesligaj and Amon [9] investigated passive thermal control using phase change materials during time-varying workloads on portable electronics. An epoxy polymer was used as a phase change material. They indicated that the operational performance of the portable electronics improved when such a passive thermal storage device was used. Pal and Joshi [10] conducted an experimental and computational study of melting in an enclosure of large aspect ratio, under a constant heat flux and discussed the effects of natural convection on the various stages of melting. Binet and Lacroix [11] conducted a numerical study of natural convection-dominated melting inside a rectangular enclosure from three discrete heat sources. A parametric study was performed to examine the effect of the cavity aspect ratio.

Lu [12] reported an analytical study of phase change cooling with an emphasis on suppressing the junction temperature rise due to transient pulses. Design guidelines for high power electronic packages were also provided. Evans et al. [13] analyzed power electronic packages and provided design guidelines relating the materials, geometry, power input and junction temperature for steady-state conditions and transient pulses.

In electronics cooling applications, transient surges in power dissipation can damage the electronics, and necessitate an effective thermal management strategy; power semiconductors are a good example of such applications. The present work considers the performance of a PCM energy storage unit under pulsed power input, and investigates the effects of different enclosure aspect ratios and locations of heat sources on the thermal energy storage process. The efficiency of the storage device is characterized using the transient variation of the peak operating temperature in the enclosure and the energy absorbed by the PCM. Careful attention is devoted to modeling the natural convection in the melt and the conjugate effects in the container walls.

## 2. MODEL FORMULATION AND NUMERICAL ANALYSIS

The problem under consideration is the melting of a pure phase change material, n-eicosane, inside a rectangular aluminum container with multiple discrete heat sources mounted on one side. A copper heat spreader is used in conjunction with the heat sources as shown schematically in Fig. 1. The liquid is assumed to be Newtonian and incompressible, and subject to the Boussinesq approximation. Thermophysical properties are assumed to remain constant over the range of temperatures considered. The volume change of the PCM during melting is neglected in this work.

In the mathematical formulation of the problem, the governing equations for mass, momentum and energy transport, respectively, are as follows:

$$\tilde{\nabla}.\tilde{U} = 0 \tag{1}$$

$$\rho\left(\frac{\partial\tilde{U}}{\partial t}+\tilde{U}\cdot\nabla\tilde{U}\right) = -\tilde{\nabla}P+\mu\tilde{\nabla}^2\tilde{U}-\frac{\mu}{K}\frac{\left(1-f_l^2\right)}{f_l^3}\tilde{U} \quad -\rho\tilde{g}\beta_T\left(T-T_0\right) \tag{2}$$

$$A(T)\frac{\partial T}{\partial t}+\tilde{\nabla}.\left[\rho\tilde{U}c_{pl}T\right] = \tilde{\nabla}.\left(k\tilde{\nabla}T\right)$$
$$A(T) = \rho c_{pl} + a(T)\ \frac{\partial f_l}{\partial T} \tag{3}$$
$$a(T) = \rho\left[\left(c_{pl}-c_{ps}\right)T+\Delta H\right]$$

In Eq. (3), A is the effective (or apparent) heat capacity [14] and accounts for the change in phase (as in [15]). To extinguish velocities in the solid region a Blake-Kozeny-Carman type source term [16] is added to the right hand side of equation (2). This source term takes a very large value in the solid region.

The phase change in the domain is modeled using the apparent heat capacity method. The key to implementing phase change in the formulation lies in specifying the change in liquid volume fraction with temperature. In principle, the relationship between the liquid fraction and temperature is given by

$$f_l=\begin{cases}1 & T>T_m\\ 0 & T\le T_m\end{cases} \tag{4}$$

Numerical algorithms are incapable of handling such a step-function and hence, the fraction of liquid and temperature should be smoothed [14]

$$f_l=\begin{cases}0 & T_p<\left(T_m-\varepsilon\right)\\ \dfrac{T_p-T_m+\varepsilon}{2\varepsilon} & \left(T_m-\varepsilon\right)\le T_p\le\left(T_m+\varepsilon\right)\\ 1 & T_p>\left(T_m+\varepsilon\right)\end{cases} \tag{5}$$

$$\frac{\partial f_l}{\partial T}=\begin{cases}0 & T_p<\left(T_m-\varepsilon\right)\\ \dfrac{1}{2\varepsilon} & \left(T_m-\varepsilon\right)\le T_p\le\left(T_m+\varepsilon\right)\\ 0 & T_p>\left(T_m+\varepsilon\right)\end{cases} \tag{6}$$

The solution of the energy equation is insensitive to the assumed variation of $f_l$ with temperature, if $\varepsilon$ is relatively small. For all the computations performed in this study, $\varepsilon_{max}$ was 0.5 K.

A uniform heat transfer coefficient is imposed on all sides, except for the side carrying the heat sources; at this wall, all the heat generated is assumed to enter the PCM unit with no losses to the ambient. An effective heat transfer coefficient was calculated for the side walls, accounting for the convective heat transfer from the fins and the base area; this value is meant to be representative of fan-cooled finned side walls, but the actual magnitude itself is somewhat arbitrary. At the start of the computations, the entire domain is at a constant initial temperature (36ºC) equal to the PCM melting temperature; the temperature of the ambient (36ºC) surrounding the unit is also considered to be constant. For the power semiconductor cooling application considered, the heat sources are assumed to be 5 mm on a side, and are equally spaced 5 mm apart. The side that carries the heat sources is 30 mm in dimension, while the other dimension (height or width depending on heat source location) is varied to set the required aspect ratio. The thickness of the copper heat spreader as well as the aluminum walls was chosen to be 1 mm. The heat input is pulsed, with each heat source dissipating 10 W as a steady-state value, rising abruptly to a transient value of 50 W per heat source. The transient pulse duration is 10 s with the pulses being separated by 300 s. The pulse separation is reduced in some cases to 150 and 30 s, as detailed in Table 1. The last two columns in Table 1 summarize the computed results.

It must be noted from Fig. 1 that the copper heat spreader is not in contact with the aluminum container walls. When calculations were performed for the heat spreader being in contact with the rest of the container, almost 60% of the heat input was transferred directly to the container walls, rather than through the very-low-conductivity PCM. Since the objective of the

present study was to characterize PCM energy storage under transient power input, the copper heat spreader and the aluminum container walls were disconnected. In practice, it would be possible to dissipate much higher power levels using this unit if the heat spreader was in intimate contact with the container walls and the PCM thermal conductivity were enhanced. In ongoing work, a PCM unit with the heat spreader in contact with the container walls is being investigated for practical applications.

The computational domain, including the enclosure walls, is discretized into finite volumes superimposed on mesh points. The field variables on the co-located grid are solved using the SIMPLE algorithm. A central differencing scheme is used for all diffusive fluxes. Since iterative solvers fail to converge when the central differencing approximation is applied to convective fluxes, a deferred correction approach [17,18] is used in this study. A fully implicit scheme (three time level scheme [18]) of second-order accuracy is used for the transient terms. The resulting coefficient matrix is solved using the Strongly Implicit Procedure. Further details of the solution procedure and discretization are available in [18, 19, 20]. For all the governing equations, iterations were terminated when the residual [18] dropped below $5 \times 10^{-6}$. The numerical code used in the present work has been previously validated and extensively benchmarked [19, 20, 21] against results in the literature for natural convection in a box, Rayleigh-Benard convection, 1-d melting problem (classical Stefan problem), directional solidification of tin, and Bridgman growth of succinonitrile. Grid independence was verified by evaluating the interface shape predicted using a series of increasingly finer meshes. For all the computations a $63 \times 63$ grid was found to be adequate. A maximum temperature difference of 0.5ºC was observed when the grid points were increased further to $92 \times 92$. More finite volumes were placed near the walls in a biased grid when the heat sources were mounted on the left wall

(configuration shown in Fig. 1). With the heat sources on the top or bottom wall, a uniform grid was employed since a multiple-cell structure needed to be resolved and steep gradients in velocity and temperature were observed in interior portions of the domain.

Numerical computations were carried out for various cases to study the effects of several parameters on the PCM energy storage unit. The parameters considered in the optimization study are listed in Table 1, while the thermophysical properties [2, 22] used are shown in Table 2. In each case, calculations were terminated either when the entire PCM in the container was completely melted, or when the heat transfer process reached a steady state.

## 3. RESULTS AND DISCUSSION

### Influence of Container Aspect Ratio

Predicted temperature, velocity and front location results are presented for a representative case in Fig. 2. The heat sources are mounted on the left wall in this case (Case 3). Initially ($\leq$ 450 s), the isotherms are planar and the melting process is dominated by conduction (results not shown). Liquid first appears adjacent to the heat spreader. The front assumes a more slanted shape as time progresses, as the rising melt carries warmer liquid towards the top. The melting interface moves faster near the top where the liquid, heated by the hot wall, impinges. As time passes, the melting spreads to adjacent regions along the walls. In the small gap between the copper heat spreader and aluminum wall, a very weak convective pattern is resolved. The bulk of the domain sees a single stable convective cell. When the pulsed heat input is supplied, the pattern is momentarily destabilized, but relaxes back to a stable pattern in the time between pulses. For Cases 1 and 2 (not shown), the thermal and velocity fields were

similar in nature, but with a less pronounced natural convection effect (due to the larger container aspect ratios).

The heat flux lost through the container walls as a function of time is shown in Fig. 3 for Case 1, with an aspect ratio of 4.0. Due to natural convection, the warm fluid rises near the heated wall and impinges on the top wall, giving rise to a greater rate of heat loss (as a flux) when compared to the right and bottom walls. The difference in heat loss between the top and bottom walls is due to the prevalent convection pattern.

The instantaneous heat absorbed by the PCM unit (difference between the heat input to the domain and the heat lost from the domain at a particular instant) is shown as a function of time in Fig. 4 for Case 1. This quantity decreases with time as the heat spreads throughout the domain and especially into the walls, increasing the heat loss from the walls. From the time that all the PCM has melted (≈ 18 mins) and a steady state has been reached (heat input = heat loss), the curve in Fig. 4 exhibits a steady behavior. The instantaneous heat absorbed decreases as time evolves due to the decrease in the available latent heat energy and the increase in the heat loss. At steady state, i.e., when the whole domain is melted, the instantaneous heat absorbed will be negligible (and only due to the specific heat).

Similar results for predicted heat loss from the domain are shown for smaller aspect ratios of 2.0 (Case 2) and 1.0 (Case 3) in Figs. 5 and 6. It is seen that for the aspect ratio of 1.0 (Fig. 6), the heat loss from the top wall is significantly higher than from the other walls, since the temperature at the right and bottom walls is much lower in this case. For the intermediate aspect ratio of 2.0 (Fig. 5), the results lie between those for the cases with aspect ratios of 4.0 and 1.0 as expected. Results such as those in Figs. 3, 5 and 6 provide design guidance regarding the

locations where internal fins may be placed in the container to enhance the PCM performance (on the right and bottom walls for an aspect ratio of 1, for example).

The variation of instantaneous heat absorbed with time for the aspect ratio of 1.0 (Case 3) is shown in Fig. 7. As for the larger aspect ratio considered in Fig. 4, the heat absorption reaches a time-independent periodic behavior by t ≈ 124 minutes, by which time all the PCM has melted for this case. The time-axis in the figure is terminated earlier to preserve clarity. It may also be noted from Figs. 4 and 7 that the heat absorbed in the interim between power pulses decreases almost linearly early in the melting process when it is conduction-dominated; at later times, as convection sets in, the heat absorbed increases during the inter-pulse periods.

## Influence of Heat Source Location

### *Heat sources mounted on bottom wall*

The influence of mounting the heat sources on the bottom wall of the PCM container is brought out in Fig. 8 where the predicted isotherms, velocity fields and melt front location are shown for Case 5 (AR = 1). The flow structure and the distribution of the convection cells would be expected to be three-dimensional in nature in this case. A Rayleigh-Benard like multiple-cell convective pattern is suggested. The melt front takes a very distinct shape with domes appearing over each convective cell where the warm fluid rises. The symmetry is lost at later times. Such observations have been reported by previous investigators as well [23,24]. It may be noted that the governing Rayleigh number is time-dependent in this case, changing as the molten region increases. Moreover, for the pulsed heating considered, the Rayleigh number is different during the pulsed versus the steady input periods. A detailed discussion of Rayleigh-Benard convection without phase change for intermediate to high Prandtl numbers (>10) can be

found in [25]. The Prandtl number considered in this study (Pr = 67.8) falls in the range of Prandtl numbers for which it has been experimentally and theoretically observed that a cross-roll instability is present, leading to bimodal convection [25]. A good review of Rayleigh-Benard convection is available in [26] and detailed numerical simulations are presented in [27,28].

As time evolves, adjacent convective cells merge together; finally coalescing into two large convective cells by the time the entire PCM has melted. After 1500 s, the melt front assumes a dome-like shape with liquid rising at the center between two counter-rotating convective cells. Based on the criterion for transition from laminar to turbulent flow reported in the literature in the absence of phase change [29], the flow field would be expected to turn turbulent at the later times.

The predicted heat loss through the container walls for this heating orientation is shown in Fig. 9 as a function of time. The heat loss through the vertical side walls is higher than that through the top wall up to approximately 60 minutes. Once the melting front makes contact with the top wall, however, heat loss through the top wall increases very rapidly and exceeds the loss through the vertical walls, as the fluid rising at the center loses most of the heat to the top wall before descending down the side walls. The whole domain took approximately 74 minutes (which includes 13 pulses) to melt completely.

***Heat sources mounted on top wall***

Figure 10 shows the predicted isotherms, velocity fields and melting front locations for a container aspect ratio of 1 with heat sources mounted on the top wall (Case 7). The heated fluid remains near the top of the domain in two stacked convective patterns due to buoyancy effects, and the interior of the PCM domain remains solid. The placement of heat sources on the top wall results in much higher temperatures along the inner edge of the heat spreader, with a

maximum predicted temperature of 66$^{o}$C (13$^{o}$C higher than for the comparable bottom heating configuration, Case 5). The melting process reached a steady state in approximately 206 minutes. Figure 11 shows that the heat is lost in this orientation mainly through the vertical side walls.

## Influence of Pulse Frequency

The transient pulsed power input to the domain was varied to study the effect on the maximum temperature attained in the domain. Two configurations, left wall and bottom wall heating, both with an aspect ratio of 1, were chosen as test cases. The transient pulses are separated by 150 s (Cases 10, 11) and 30 s (Case 12) with the amount of heat input being the same as before (10 W steady and 50 W pulse per heat source). Figure 12 shows a comparison of the maximum temperatures in the domain as a function of time with the different pulsed inputs for heating at the left wall. For Case 12, since the entire domain melts in 17 minutes, a more detailed comparison in shown in Fig. 13. Results in these two figures show that a reduction in pulse frequency from 300 to 150 s has a negligible effect on the maximum temperature in the domain. The convection in both these cases damps out the pulses rapidly. Case 12, on the other hand, experiences higher temperatures in comparison, since the pulses are much closer together. The total heat input to the phase change storage system in any given period is also much higher in Case 12 than in Cases 3 and 10. It is hence the cumulative effect of the higher heat input to the system along with the increased pulse frequency which increases the maximum temperature observed in the PCM unit in Case 12. It is clear from Fig. 13 that significant differences in temperature exist between Cases 3 and 12 at the end of the relaxation times (just before a new pulse is applied).

Similar results for the effect of pulse frequency on the maximum temperatures for bottom wall heating are shown in Fig. 14, where Cases 5 and 11 are compared. Again, it is seen that a reduction in pulse frequency from 300 to 150 s does not result in significant differences in maximum temperatures.

## Performance of the Thermal Energy Storage Unit

Figure 15 shows the cumulative heat energy absorbed by the thermal storage device with time. Amongst all the cases considered in this study (all are not shown in the figure for clarity), Case 5 (bottom heating, AR = 1) displays the highest thermal storage capacity. For the heat sources mounted on the left wall, Cases 3 and 4 (AR = 1 and 0.5) exhibit similar performance with respect to energy storage. Cases 1, 2, 6, 9 and 12 reach a steady state very early for different reasons and offer limited energy storage. Placing heat sources on the top wall (Cases 7, 8) is clearly not beneficial from a thermal storage standpoint.

The peak operating temperatures are also compared for several cases in Fig. 16. Case 5 (bottom heating, AR = 1) clearly emerges as the best choice for maintaining the lowest peak temperatures. For the heat sources mounted on the left wall, the peak operating temperatures for all aspect ratios followed more or less the same trend and fell between the range shown for the top and bottom heating cases in Fig. 16.

For an input power pulse spacing of 300 s, the pulse spacing appears to be large enough for the peak operating temperatures to decay to an equilibrium value before a successive pulse is applied, for all cases. Reducing this pulse spacing to 30 s results in the pulses having a cumulative effect on the peak operating temperatures.

## 4. CONCLUSIONS

A fully transient analysis of the phase change process inside a rectangular enclosure was carried out for electronics cooling applications with pulsed power dissipation. The influence of changes in the frequency of pulses, heat source location and aspect ratio of the containment volume on the thermal performance of the PCM unit was studied. The performance of the latent heat energy storage device was quantified by studying the cumulative heat energy absorbed, maximum temperature observed in the container, heat loss through the container walls and instantaneous heat absorbed.

The heat source location and container aspect ratio play a very significant role in the performance of the PCM energy storage unit considered. Among the configurations investigated, the PCM unit with heat sources located on the bottom wall had the best thermal performance, with a higher rate of heat absorption and lower average maximum temperatures.

It would be beneficial to enhance the thermal response of the phase change material itself to better handle sudden spikes in power dissipation. In ongoing work, enhancement of the thermal conductivity of the PCM using internal fins and porous metal foams is being investigated, along with experimental validation of the numerical predictions being developed. With enhanced PCM conductivity, the effects of heat source location on the performance of the unit found in this study are expected to be less pronounced.

### Acknowledgement

Funding for this work from industry members of the Purdue NSF Cooling Technologies Research Center (http://widget.ecn.purdue.edu/~CTRC) is gratefully acknowledged.

## REFERENCES


1 S. Himran, A. Suwono and G. A. Mansoori, “Characterization of Alkanes and Paraffin Waxes for Application as Phase Change Energy Storage Medium,” Energy Sources, vol. 16, pp. 117-128, 1994.

2 W. R. Humphries and E. L. Griggs, “A Design Handbook of Phase Change Thermal Control and Energy Storage Devices,” NASA TP 1074, 1974.

3 S. M. Hasnain, “Review of Sustainable Thermal Storage Technologies, Part I: Heat Storage Materials and Techniques,” Energy Conversion Management, vol. 39, pp. 1127-1138, 1998.

4 M. Ishizuka and Y. Fukuoka, “Development of a New High Density Package Cooling Technique using Low Melting point Alloys,” Proceedings of ASME/JSME Joint Thermal Engineering Conference, vol. 2, pp. 375-380, 1991.

5 K. W. Baker, J. H. Jang and J. S. Yu, “Thermal Control of Phase Change Package with Periodic Pulse Heating - A Case Study,” Proceedings ASME/JSME Joint Thermal Engineering Conference, vol. 4, pp. 463-469, 1995.

6 D. Pal and Y. Joshi, “Application of Phase Change Materials for Passive Thermal Control of Plastic Quad Packages: A Computational Study,” Numerical Heat Transfer, Part A, vol. 30, pp. 19-34, 1996.

7 D. Pal and Y. Joshi, “Application of Phase Change Materials to Thermal Control of Electronic Modules: A Computational Study,” Journal of Electronic Packaging, vol. 119, pp. 40-50, 1997.

8 E. M. Alawadhi and C. H. Amon, “Performance Analysis of an Enhanced PCM Thermal Control Unit,” Proceedings of ITherm 2000, pp. 283-289, 2000.

9 M. J. Vesligaj and C. H. Amon, “Transient Thermal Management of Temperature Fluctuations during Time Varying Workloads on Portable Electronics,” IEEE Transactions on Components and Packaging Technology, Vol. 44, pp. 1619-1625, 1999.

10 D. Pal and Y. Joshi, “Melting In A Side Heated Tall Enclosure By A Uniformly Dissipating Heat Source,” International Journal of Heat and Mass Transfer, vol. 44, pp. 375-387, 2001.

11 B. Binet and M. Lacroix, “Melting From Heat Sources Flush Mounted On A Conducting Vertical Wall,” International Journal of Numerical Methods in Heat Fluid Flow, vol.10, pp. 286-303, 2000.

12 T. J. Lu, “Thermal Management of High Power Electronics with Phase Change Cooling,” International Journal of Heat and Mass Transfer, Vol. 43, pp. 2245-2256, 2000.

13 A. G. Evans, M. Y. He, J. W. Hutchinson, and Shaw, M., "Temperature Distribution in Advanced Power Electronics Systems and the Effect of Phase Change Materials on Temperature Suppression during Power Pulses," Journal of Electronics Packaging, Vol. 123, pp. 211-217, 2001.

14 J. A. Dantzig, "Modeling Liquid-Solid Phase Changes with Melt Convection," International Journal of Numerical Methods in Engineering, Vol. 28, pp. 1769-1785, 1989.

15 X. Zeng and A. Faghri, "Temperature-Transforming Model For Binary Solid-Liquid Phase Change Problems. Part 1: Mathematical Modeling," Numerical Heat Transfer, Part B, vol. 25, pp. 467-480, 1994.

16 A. D. Brent, V. R. Voller and K. J. Reid, "Enthalpy-Porosity Technique for Modeling Convection-Diffusion Phase Change: Application of the Melting of a Pure Metal, " Numerical Heat Transfer, vol. 13, pp. 297-318, 1988.

17 P. K. Khosla, and S. G. Rubin, "A Diagonally Dominant Second-Order Accurate Implicit Scheme," Computers Fluids, Vol. 2, pp. 207-209, 1974.

18 J. H. Ferziger and M. Peric, *Computational Methods for Fluid Dynamics*, Springer-Verlag, Berlin, 1996.

19 J. E. Simpson, S. V. Garimella, H. C. de Groh III and R. Abbaschian, "Bridgman Crystal Growth of an Alloy with Thermosolutal Convection under Microgravity Conditions," Journal of Heat Transfer, vol. 123, pp. 990-998, 2001.

20 J. E. Simpson and S. V. Garimella, "An Investigation of the Solutal, Thermal and Flow Fields in Unidirectional Alloy Solidification," International Journal of Heat and Mass Transfer, vol. 41, pp. 2485-2502, 1998.

21 J. E. Simpson, Garimella, S. V., and H. de Groh III, " An Experimental and Numerical Investigation of the Bridgman Growth of Succinonitrile," AIAA Journal of Thermophysics and Heat Transfer, Vol. 16, pp. 324-335, 2002.

22 F. P. Incropera and D. P. DeWitt, *Fundamentals of Heat and Mass Transfer*, John Wiley & Sons, New York, 1998.

23 L. A. Diaz and R. Viskanta, "Visualization of the Solid-Liquid Interface Morphology formed by Natural Convection during Melting of a Solid from below," International Communication of Heat and Mass Transfer, vol. 11, pp. 35-43, 1984.

24 Z. Gong and A. Majumdar, "Flow and Heat Transfer in Convection Dominated Melting in a Rectangular Cavity Heated from Below," International Journal of Heat and Mass Transfer, vol. 41, pp. 2573-2580, 1998.

25 F. Stella, G. Guj and E. Leonardi, “The Rayleigh-Benard Problem in Intermediate Bounded Domains,” Journal of Fluid Mechanics, Vol. 24, pp. 375-400, 1993.

26 K. T. Yang, “Transitions and Bifurcations in Laminar Buoyant flows in Confined Enclosures,” Journal of Heat Transfer, Vol. 110, pp. 1191-1204, 1988.

27 D. Mukutmani and K. T. Yang, “Rayleigh-Benard Convection in a Small Aspect Ratio Enclosure: Part I – Bifurcations to Oscillatory Convection,” Journal of Heat Transfer, Vol. 115, pp. 360-366, 1993.

28 D. Mukutmani and K. T. Yang, “Rayleigh-Benard Convection in a Small Aspect Ratio Enclosure: Part II – Bifurcations to Chaos,” Journal of Heat Transfer, Vol. 115, pp. 367-376, 1993.

29 J. S. Turner, *Buoyancy Effects in Fluids*, Cambridge Press, London, 1973.

Table 1: Geometrical and Thermal Parameters.

| Case | Times for 10 & 50 W Inputs (s) | Aspect Ratio† | Heat Source Location | PCM Total Melting Time (min) | Peak Temp. (°C) |
|---|---|---|---|---|---|
| 1 | 300-10 | 4.0 | Left | 18 | 57.5 |
| 2 | 300-10 | 2.0 | Left | 47 | 57.8 |
| 3 | 300-10 | 1.0 | Left | 124 | 57.2 |
| 4 | 300-10 | 0.5 | Left | 219# | 56.3 |
| 5 | 300-10 | 1.0 | Bottom | 74 | 53.0 |
| 6 | 300-10 | 4.0 | Bottom | 10 | 54.2 |
| 7 | 300-10 | 1.0 | Top | 206# | 65.7 |
| 8 | 300-10 | 1.5 | Top | 196 | 61.4 |
| 9 | 300-10 | 4.0 | Top | 16 | 63.9 |
| 10 | 150-10 | 1.0 | Left | 86 | 57.1 |
| 11 | 150-10 | 1.0 | Bottom | 63 | 52.7 |
| 12 | 30-10 | 1.0 | Left | 17 | 60.0 |

# - Attained steady state with solid remaining in domain
† - Ratio of the dimension of the side carrying the heat sources to the dimension of the perpendicular side

Table 2: Thermophysical Properties [2,22].

| Property | Eicosane | Copper | Aluminum |
|---|---|---|---|
| Thermal Conductivity (W/mK) | 0.1505 | 401.0 | 244.0 |
| Specific Heat (kJ/kgK) | 2.46 | 0.385 | 0.903 |
| Density (kg/m$^3$) | 769 | 8933 | 2702 |
| Latent Heat of Fusion (kJ/kg) | 247.3 | - | - |
| Dynamic Viscosity (g/ms) | 4.15 | - | - |
| Coeff. of Thermal Expansion (K$^{-1}$) | $8.5\times10^{-4}$ | - | - |
| Melting Temp. (°C) | 36 | - | - |

## List of Figures

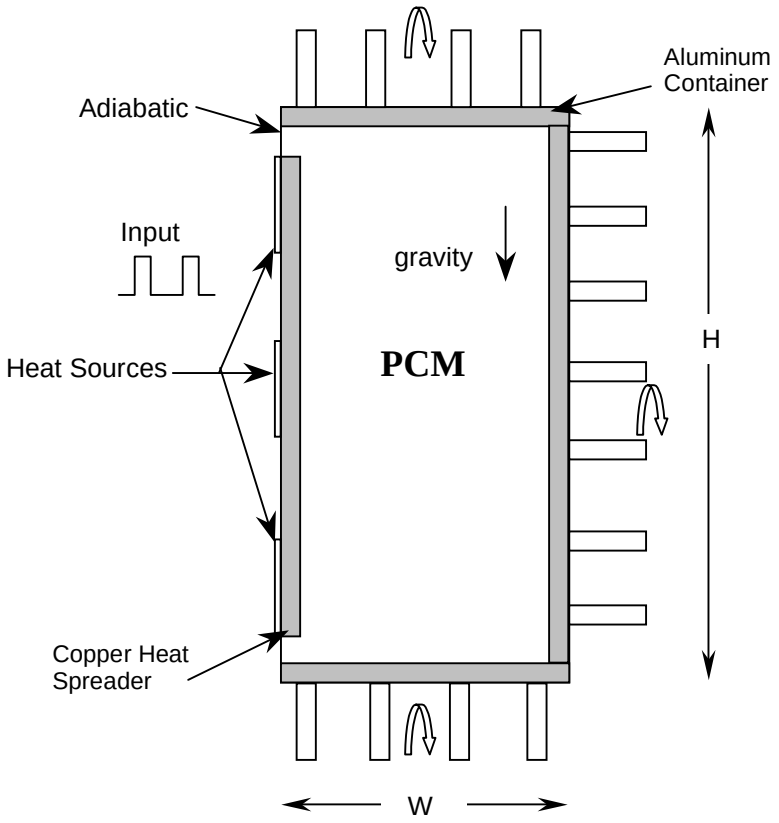


Fig. 1: Schematic of the PCM energy storage unit investigated in the present study.

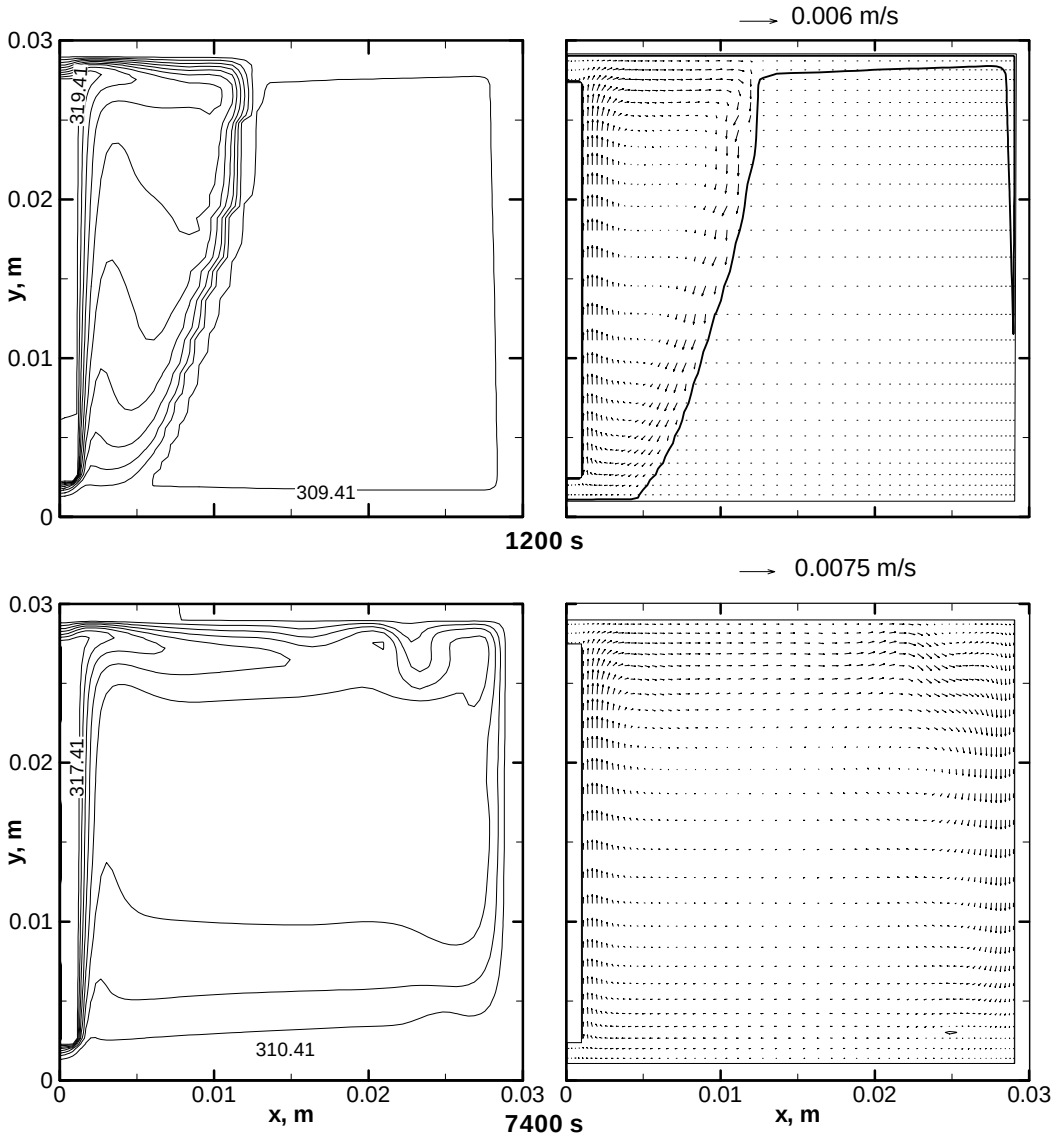


Fig. 2: Predicted isotherms (left), velocities (right) and melt front locations for an aspect ratio of 1.0 (Case 3). Isotherms are shown in equal increments.

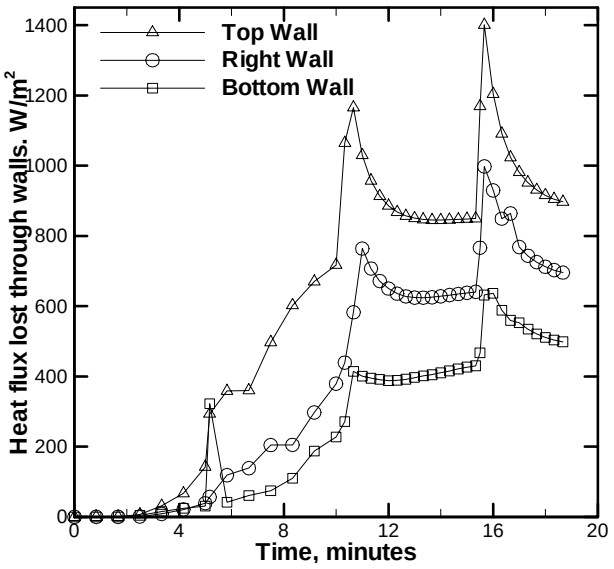


Fig. 3: Heat lost from the walls of the container as a function of time for an aspect ratio of 4.0 (Case 1).

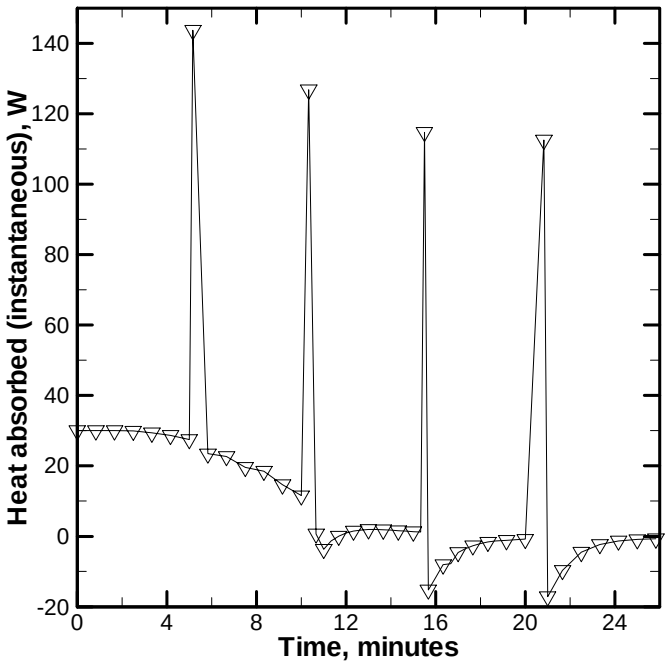


Fig. 4: Instantaneous heat absorption into the PCM unit for an aspect ratio of 4.0 (Case 1).

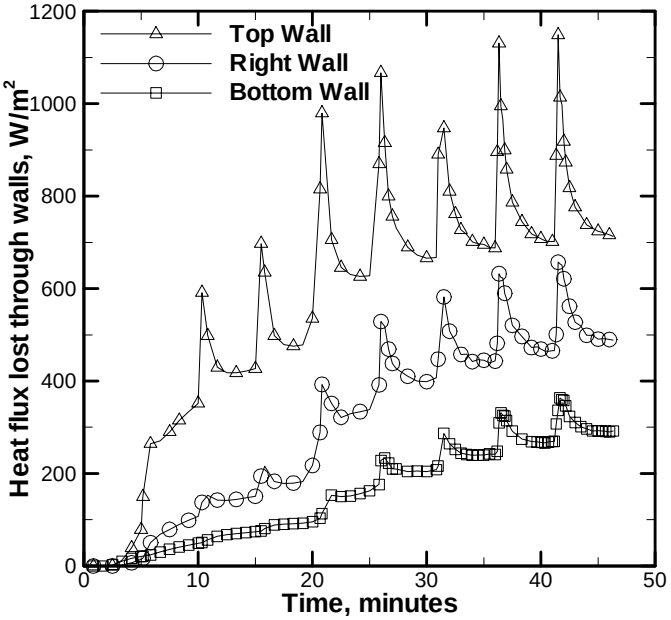


Fig. 5: Heat lost from the container walls as a function of time for an aspect ratio of 2.0 (Case 2).

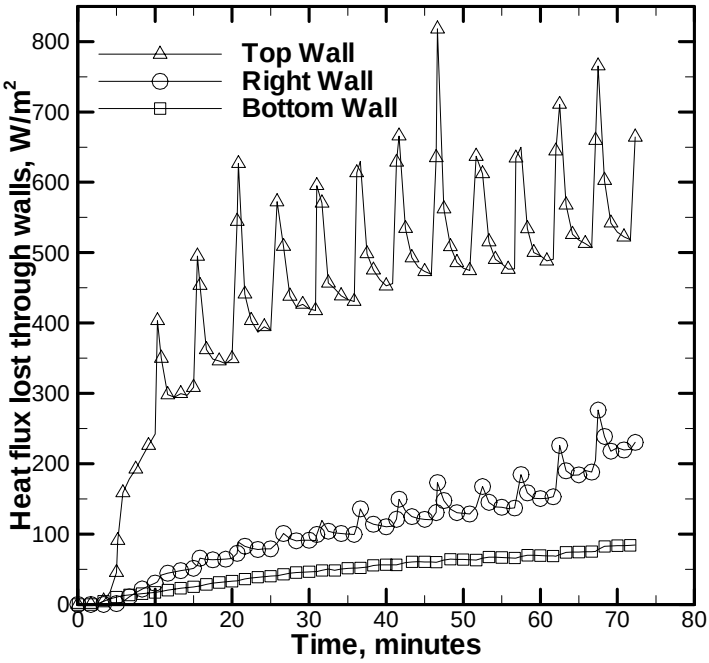


Fig. 6: Heat lost from the container walls as a function of time for an aspect ratio of 1.0 (Case 3).

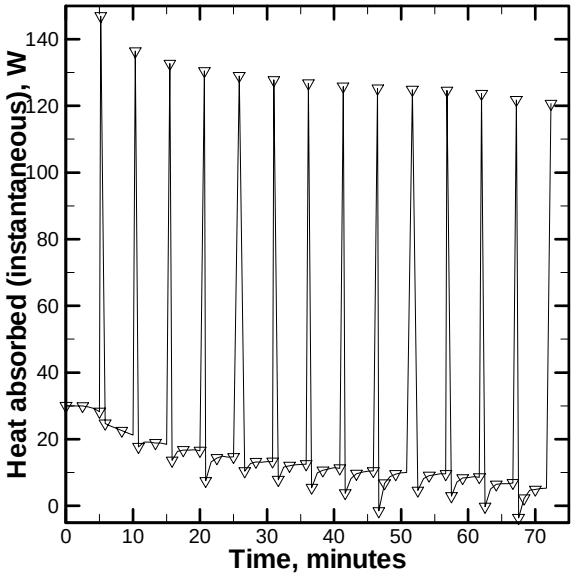


Fig. 7: Instantaneous heat absorption into the PCM unit for an aspect ratio of 1.0 (Case 3).

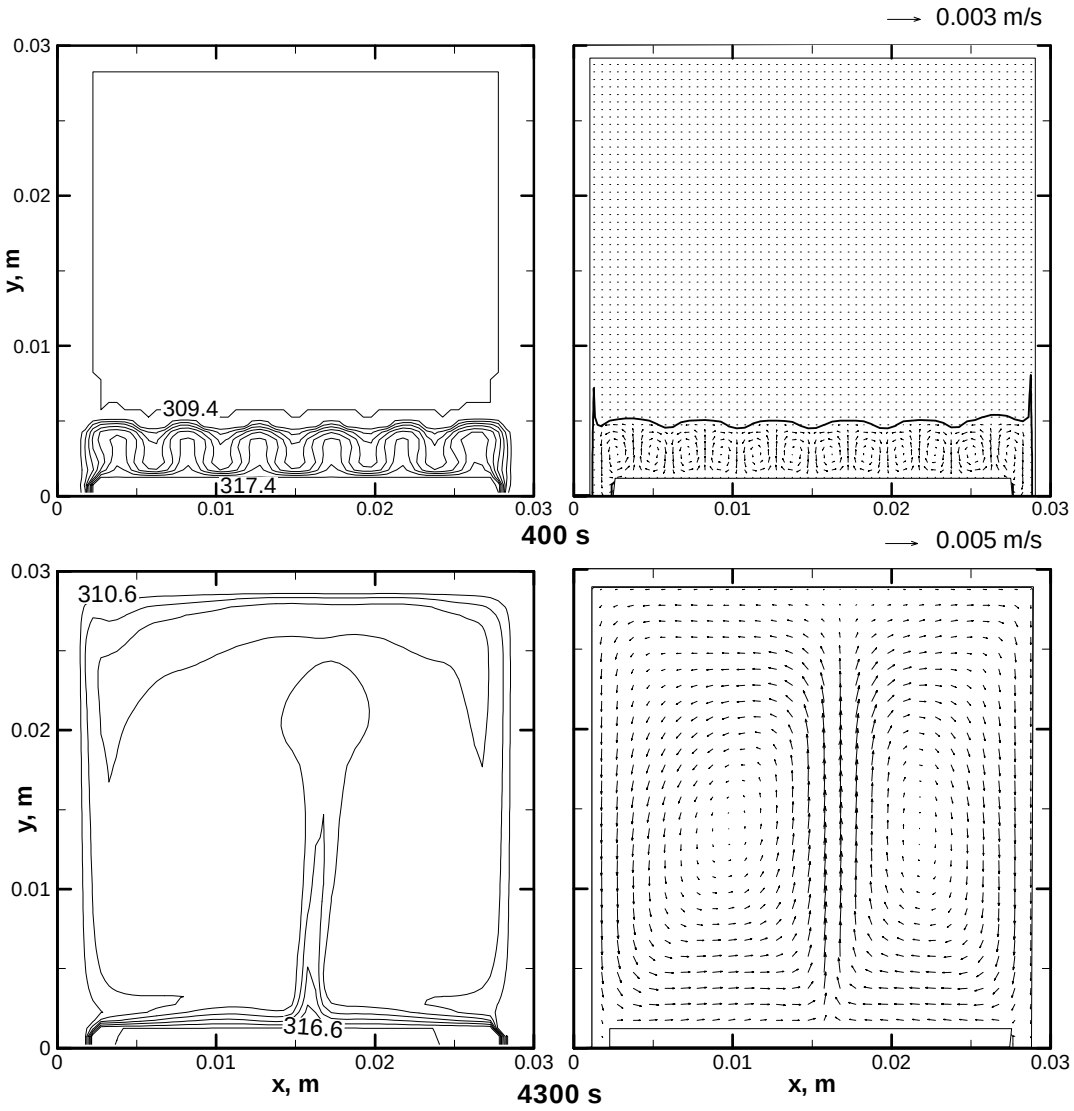


Fig. 8: Predicted temperature and velocity fields for Case 5 with front locations for aspect ratio = 1.0 (Isotherms are in equal increments).

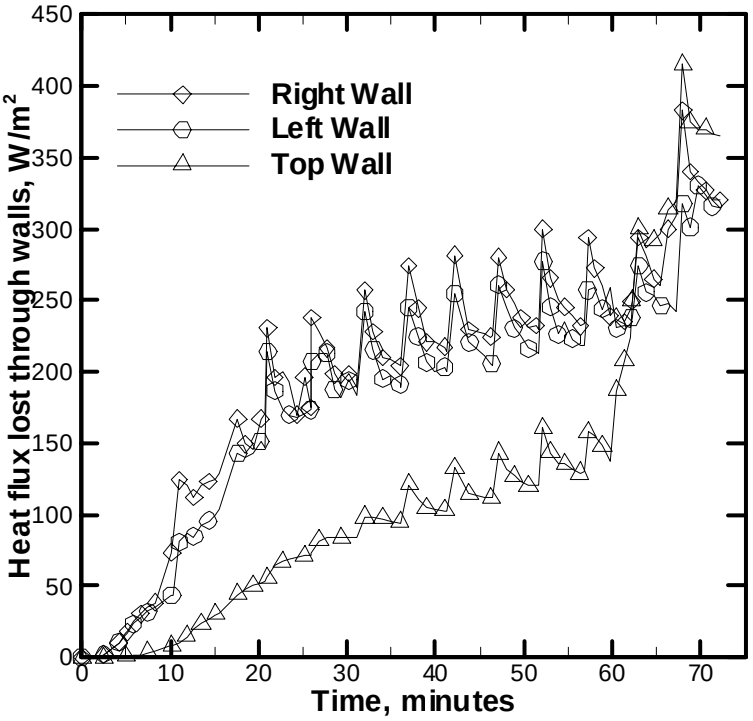


Fig. 9: Heat lost from the container walls as a function of time for aspect ratio = 1.0 (Case 5).

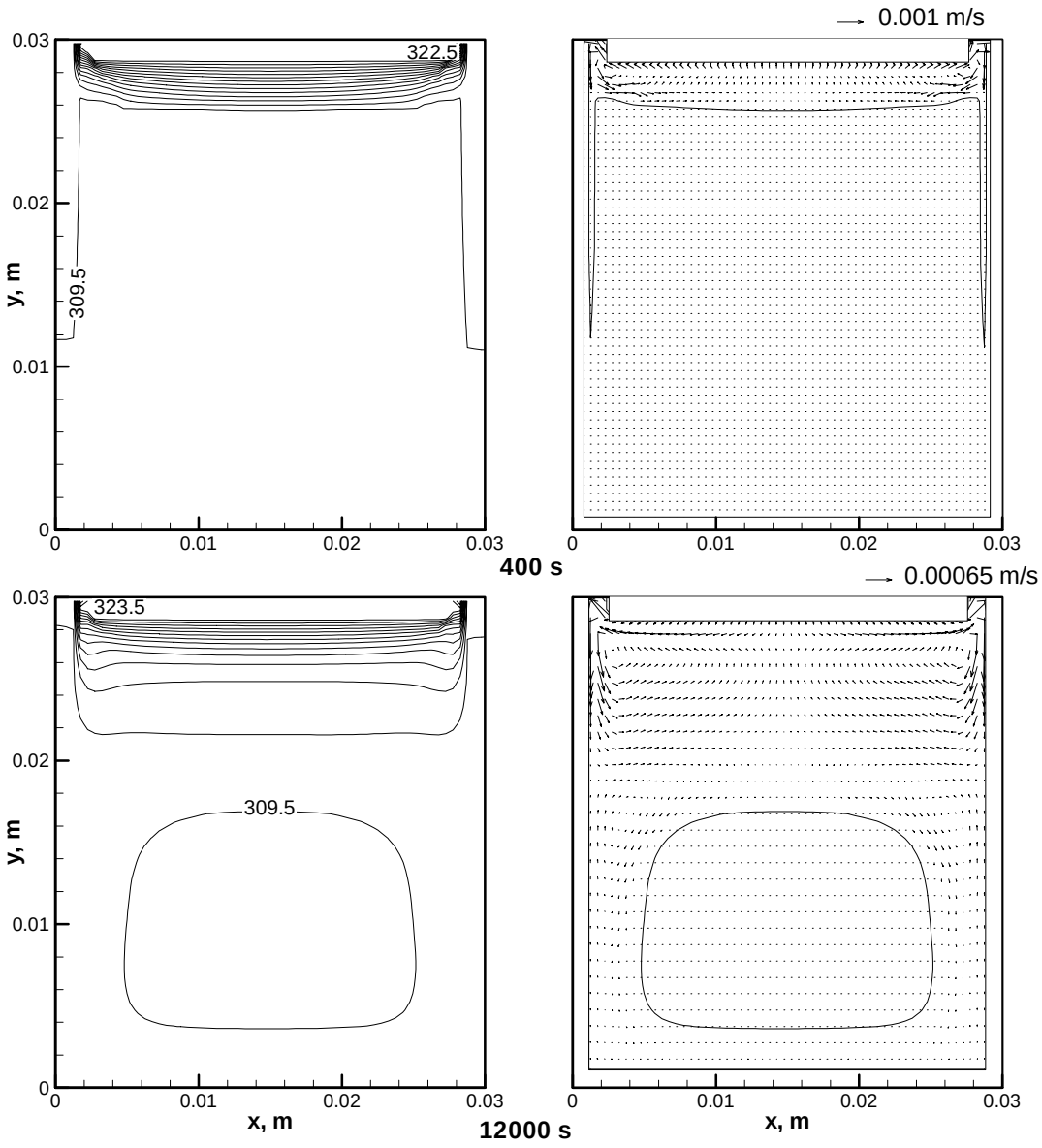


Fig. 10: Predicted temperature and velocity fields for an aspect ratio of 1 (Case 7) along with front locations (isotherms are shown in equal increments).

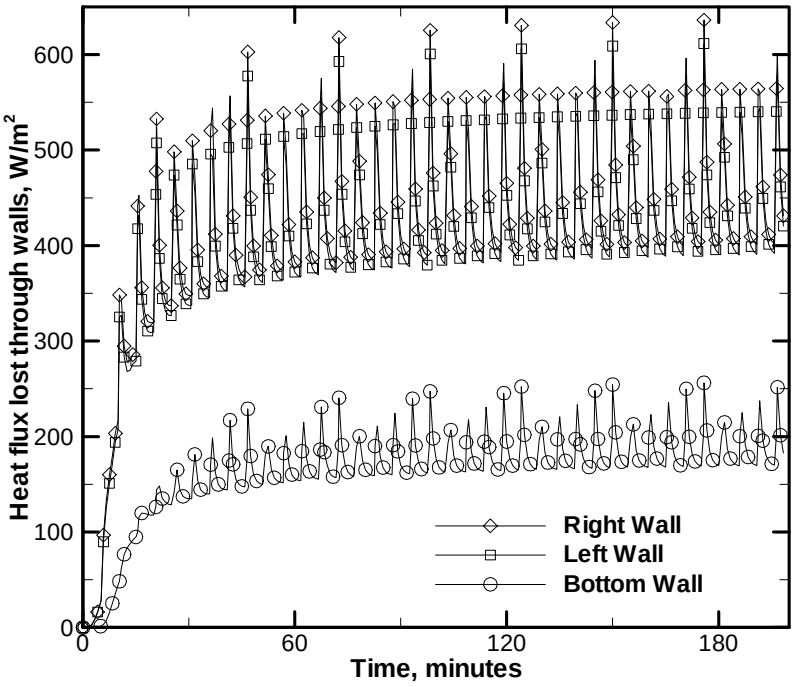


Fig. 11: Heat lost from the container walls as a function of time for aspect ratio = 1.0 (Case 7).

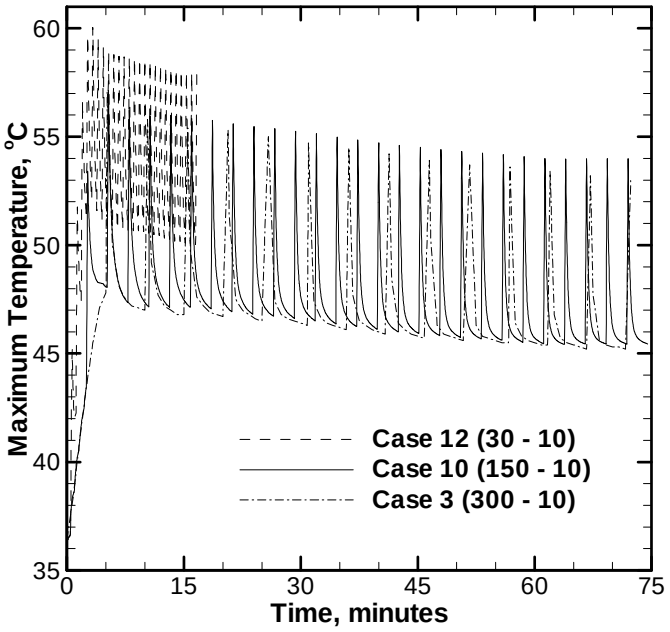


Fig. 12: Temporal variation of maximum temperature in the domain for an aspect ratio of 1.0 with the left wall heated (Cases 3, 10, 12).

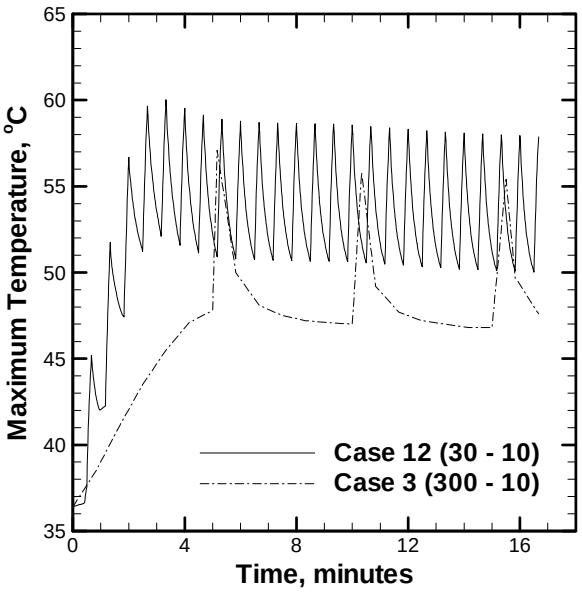


Fig. 13: Details of the variation of maximum temperature in the domain for an aspect ratio of 1.0 (Case 12,3).

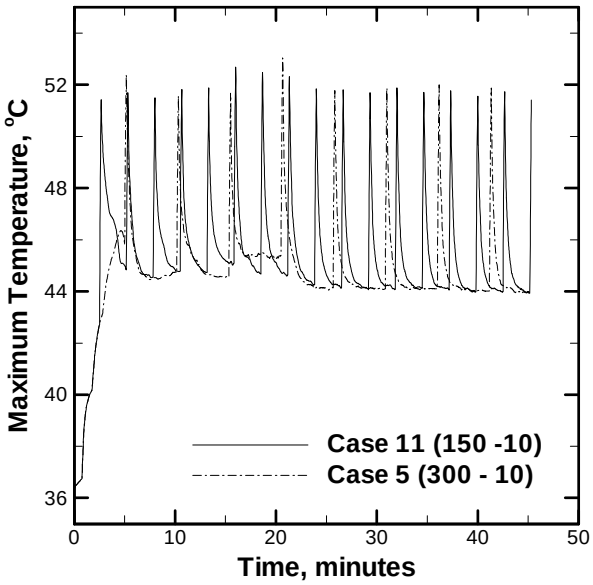


Fig. 14: Maximum temperature as a function of time for an aspect ratio of 1.0 with the bottom wall heated (Cases 11,5).

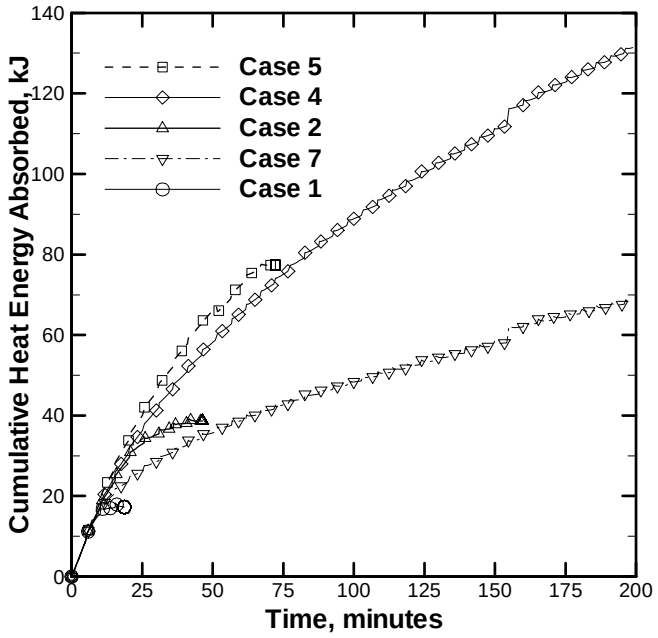


Fig. 15: Comparison of cumulative heat energy absorbed with time for different configurations.

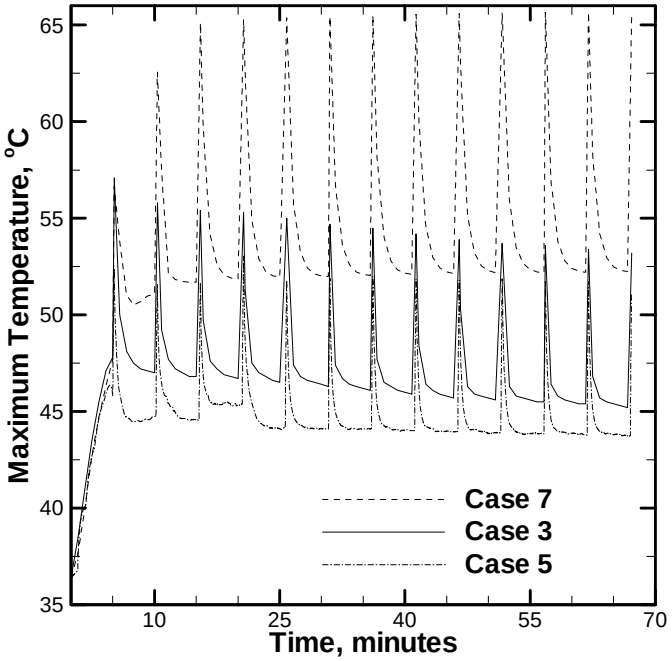


Fig. 16: Comparison of peak operating temperature as a function of time for top, left and bottom heating, with pulses separated by 300 s (other cases left out for clarity).